

Article

In Silico Structural and Functional Analysis of the Mitochondrial Malate Transporters in Oleaginous Fungus *Mucor circinelloides* WJ11

Wu Yang^{1,2}, Hassan Mohamed^{1,3,*} , Aabid Manzoor Shah¹, Huaiyuan Zhang¹, Shuxian Pang¹, Wenye Shi¹, Futing Xue¹ and Yuanda Song^{1,*} 

¹ Colin Ratledge Center for Microbial Lipids, School of Agricultural Engineering and Food Science, Shandong University of Technology, Zibo 255049, China

² School of Biology and Brewing Engineering, Taishan University, Taian 271000, China

³ Department of Botany and Microbiology, Faculty of Science, Al-Azhar University, Assiut 71524, Egypt

* Correspondence: hassanmohamed85@azhar.edu.eg (H.M.); ysong@sdut.edu.cn (Y.S.);
Tel.: +86-156-5330-1370 (H.M.); +86-139-0617-4047 (Y.S.)

Abstract: Malate transporter proteins (MTPs) play a pivotal role in regulating flux in the citrate/malate/pyruvate shuttle to deliver acetyl-CoA from the mitochondria to the cytosol and thus regulate lipid biosynthesis in oleaginous fungi. Despite the recent successful exploration of the mitochondrial malate transporters in *Mucor circinelloides*, research with *in silico* analyses that include molecular docking and their dynamics, in addition to homology modelling of malate transporters, have not been reported. In this study, the physico-chemical properties and nucleotide sequence analysis of two mitochondrial MTPs (MT and SoDIT-a with Gene/protein ID scaffold00018.48 and scaffold00239.15, respectively), in *M. circinelloides* WJ11 were performed. The three-dimensional (3D) model of the mitochondrial MTPs was determined and the best-docked complex stabilities were demonstrated with molecular dynamic (MD) simulations. The activity domain was revealed to form hydrogen bonds and piling interactions with citrate and malate upon docking. Our study showed better binding affinities for the MTPs—reaching up to -3.44 and -7.27 kcal/mol with the MT and SoDIT-a proteins, respectively (compared to the target of -2.85 and -6.00 kcal/mol for citric acid-binding). MD simulations illustrated that the protein complexes demonstrated conformational stability throughout the simulation. This study was the first to elucidate the structural characteristics of mitochondrial MTPs in *M. circinelloides* WJ11, providing direct evidence regarding the transport mechanism of specific substrates. Furthermore, the current results support ongoing efforts to combine functional and structural data to better understand the MTPs (at the molecular and atomic levels) of an oleaginous fungus such as *M. circinelloides*.

Keywords: *Mucor circinelloides*; malate transporter; molecular modelling; molecular dynamics



Citation: Yang, W.; Mohamed, H.; Shah, A.M.; Zhang, H.; Pang, S.; Shi, W.; Xue, F.; Song, Y. *In Silico* Structural and Functional Analysis of the Mitochondrial Malate Transporters in Oleaginous Fungus *Mucor circinelloides* WJ11. *Catalysts* **2023**, *13*, 705. <https://doi.org/10.3390/catal13040705>

Academic Editor: Evangelos Topakas

Received: 13 March 2023

Revised: 31 March 2023

Accepted: 3 April 2023

Published: 6 April 2023



Copyright: © 2023 by the authors. Licensee MDPI, Basel, Switzerland. This article is an open access article distributed under the terms and conditions of the Creative Commons Attribution (CC BY) license (<https://creativecommons.org/licenses/by/4.0/>).

1. Introduction

All organisms synthesise lipids to create and maintain permeable cell membranes and organelles [1]; however, oleaginous microorganisms can furthermore accumulate large amounts of lipids (representing more than 20% (*w/w*) of their biomass). This is possible due to a reverse beta-oxidation reaction (in nitrogen-restricting conditions) which results in a continuous provision of acetyl-CoA and NADPH and thus allows for the production of fatty acids (FAs) [2,3]. It is known that, in some filamentous fungi, mitochondrial membrane shuttle proteins assist with the effective transport of organic acids [4]. For example, mitochondrial, and cytoplasmic malate transporter (MT) proteins are responsible for the transport of malate across these respective membranes and for binding malate metabolism to different sub-cellular areas. Whilst malate can serve as an energy and carbon source for microbial growth, the importance of this dicarboxylic acid in the tricarboxylic

acid (TCA) cycle and its role in central metabolic pathways makes it one of the most promising building block chemicals [5].

The transporters of malate have been proven as essential for FA biosynthesis in oleaginous microorganisms [6]. The conversion of malate to pyruvate (via a cytosolic malic enzyme (ME)) plays a vital role in the generation of NADPH, which in turn promotes the elongation and desaturation reactions of polyunsaturated fatty acids (PUFAs) and sterols [6,7]. Some studies using oleaginous *Mucor circinelloides* and *Mortierella alpina* strains have over-expressed ME for better malate-to-pyruvate catalysis and subsequent lipid over-accumulation [8,9]. Similarly, MT overexpression in *M. circinelloides* has been deemed a successful approach to studying malate-associated lipid biosynthesis [10]. Various studies have thus highlighted the potential of MTs (and malate) in FA biosynthesis including the finding that increased levels of malate in the cytosol can affect citrate efflux by serving as a counter-substrate for citrate and isocitrate [11]. In our recent study based on genomic mapping of *Mucor circinelloides* WJ11, five transporter genes (i.e., one MT, one tricarboxylate carrier (TCT), one citrate transport protein (CT), and two 2-oxoglutarate/malate antiporters (SoDIT-a and SoDIT-b)) had been detected [12]. Previously, we have illustrated that an MT expressed in *M. circinelloides* strain CBS 277.49 efficiently regulated malate flux and resulted in lipid over-accumulation [10]. To adequately study the functions of multiple proteins, both computational and ligand-binding methods are needed. Many bioinformatics tools have thus been developed to anticipate ligand-binding positions as an initial step to understand protein function or to aid with docking computations and potential interaction-based screening analysis [13]. Yet, no modelling studies or binding characterisations have been assessed for MTs during lipid accumulation in filamentous fungi.

To gain a better understanding of MT protein functions in the mitochondrial malate transport system, general features such as protein sequence identity, domain structures, and validations were studied *in silico*. Our study confirmed that MT proteins contribute to the efflux of malate from the mitochondria—providing a sufficient carbon source for cell utilisation and thereby playing a significant role in lipid accumulation.

2. Results and Discussion

2.1. Nucleotide Sequence and Phylogenetic Analysis

The protein sequences of MT and SoDIT-a (i.e., gene/protein ID scaffold00018.48 and scaffold00239.15) were obtained via UniProt and were used for *in silico* analyses. Both represented mitochondrial carrier proteins with 90.6% (MT) and 66% (SoDIT-a) BLAST sequence identities. This meant that proper templates for protein homology modelling were unavailable. A phylogenetic tree, constructed using the neighbour-joining method in MEGA6.0, had been provided previously [12]. Additionally, ClustalW multiple sequence alignments were employed to demonstrate sequence homology with other mitochondrial malate transporters. Ten protein structures (with a higher Z-score) were selected as template structures for subsequent modelling calculations. The templates of the MT and SoDIT-a proteins were highly similar in their topology, although with different chain structures and stacking of the same protein (Figure 1a,b). Among them, two templates had a high similarity to 3m71 and 4f35 and were selected as secondary structure prediction templates for the MT and SoDIT-a proteins. The sequence identities between the 3M71 and MT protein targets with their best templates were estimated to be 21%, and the sequence identities between 4F35 and SoDIT reached up to 19%.

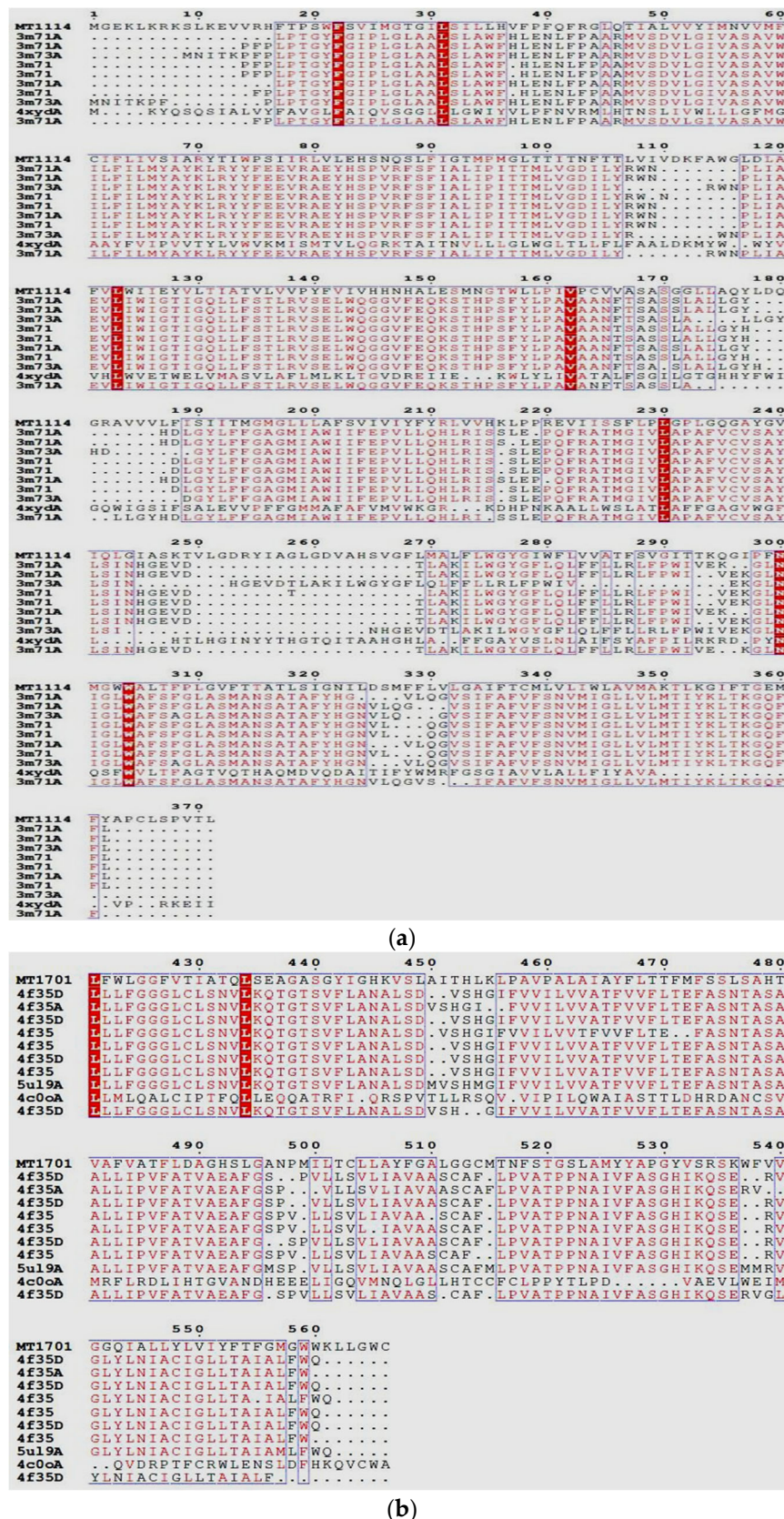


Figure 1. Multiple sequence alignment of (a) MT with an accession number KQ435319.1 and (b) SoDIT-a protein with an accession number KQ435538.1. Blue boxes indicate similar regions, red sequences within the boxes indicate sequences that are consistent with the comparison results, and red underlining indicates conserved loci.

2.2. Physico-Chemical Properties of Target Proteins

The physico-chemical properties of the studied genes were determined by the analogous properties of their amino acids. The MT and SoDIT-a proteins were composed of 371 and 566 amino acid residues, respectively, with a corresponding molecular mass of 40.99 and 60.62 kDa. The MT and SoDIT-a proteins, respectively, contained 7.3% and 8% positively charged amino acid residues (Arg⁺, His⁺, and Lys⁺), in addition to 3.5% and 5.8% negatively charged amino acid residues (Asp⁻ and Glu⁻). The pI values were calculated to be 9.16 (MT) and 6.56 (SoDIT-a), which indicated that the tested proteins were, respectively, alkaline and neutral, whilst low instability index values, i.e., 23.34 (MT) and 35.35 (SoDIT-a), predicted that these proteins were stable. Aliphatic index analyses of the MT and SoDIT-a protein sequences indicated that leucine was found to be the most frequent amino acid (14.0 and 13.6%, respectively), followed by valine (11.3%), serine (10.1%), isoleucine (10.0%), and alanine (9.5%). The GRAVY (hydropathy) values of 1.080 (MT) and 0.599 (SoDIT-a) indicated better interaction of MT and SoDIT-a proteins with the surrounding water molecules.

The MT and SoDIT-a proteins were thus found to be small proteins with a lower number of charged amino acid residues between their bi-layer, whereas the highly hydrophobic amino acid residues were embedded through the transmembrane layer, which in turn allowed for stable interaction with a non-polar lipid membrane. The proteins showed a high hydrophobicity of 86.2% (MT) and 69.7% (SoDIT-a) (Supplementary Material Figure S1), allowing for the efficient transport of molecules across the membrane (serving as a membrane barrier function and protein embedding platform).

2.3. Homology Modelling and Validation

The I-TASSER-based 3D structural models and experimentally detected structures of the MT and SoDIT-a proteins are presented in Figure 2. Generally, the structural model of the MT protein had been roughly similar in fold/topology to the native protein and presented as a typical transmembrane protein channel (formed by the winding of helical chains) with a cylindrical hollow structure—features that could be useful for domain classification and family assignment (Figure 2a,b). The SoDIT-a protein structure presented as a transmembrane protein channel (formed by the assembly of helical chains and randomly coiled aggregates) with the presence of molecular channels in the structural domain leading to smooth molecular transport (Figure 2c,d). The C-scores of the tested proteins highly correlated with the accuracy of the I-TASSER models and the experimental structures. As the crystal structures of these MT and SoDIT-a proteins have not yet been reported, the plausibility and accuracy of our generated data required further verification. Therefore, PROCHECK and ERRAT analyses of the target MT and SoDIT-a models were performed. The selection of the final model candidates was based on Ramachandran Plot (using RAMPAGE) analyses and PROCHECK stereo-chemical characteristics (i.e., having the highest number of residues in appropriate sites whilst having the lowest number of residues in disapproved regions).

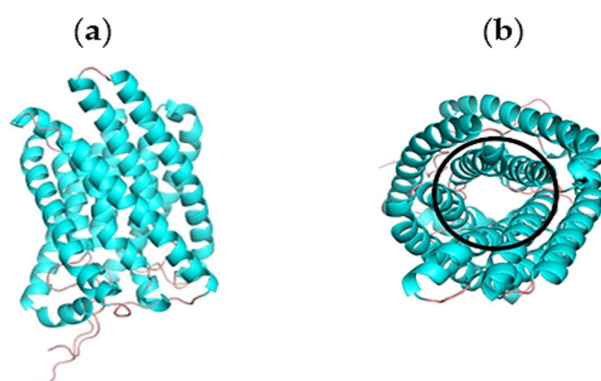


Figure 2. Cont.

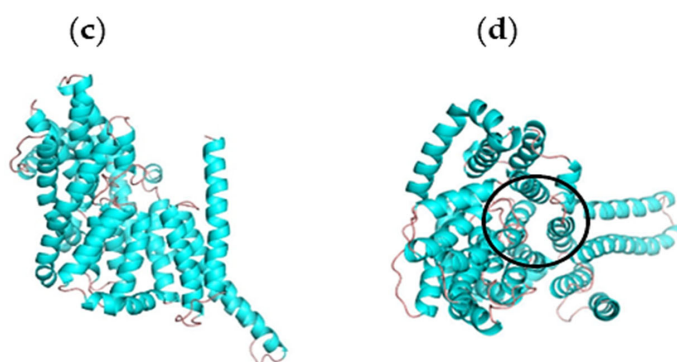


Figure 2. Predicted 3D structure models of target proteins. (a) Side view and (b) top view of the MT model, as well as (c) side view and (d) top view of the SoDIT-a model.

Based on the high homology of the MT and SoDIT-a templates (specifically 3M71 and 4F35), multimeric structural models of these proteins could be predicted according to their high similarity templates. These two templates were subsequently optimised using GROMACS 4.6 kinetics software, and the results showed that the two subunits of the target proteins were well-matched in spatial summation. Furthermore, the lateral helical chain surfaces of the subunits were non-polar regions and/or regions with little positive charge, which may lead to an increase in hydrophobicity and may facilitate aggregation between these sub-units (as shown in Figure 3).

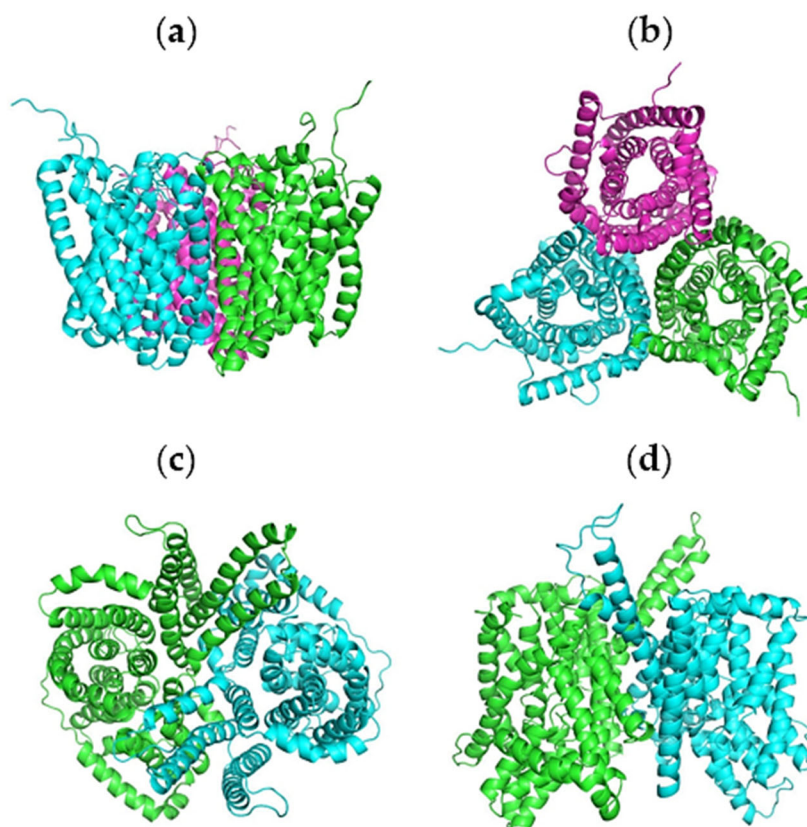


Figure 3. The 3D structure of target protein multimeric forms. (a) Side view and (b) top view of the MT model, as well as (c) side view and (d) top view of the SoDIT-a model from *M. circinelloides* WJ11.

The final models were selected as described above (Figure 4a,b). Our RAMPAGE analyses revealed that 93.9% of the amino acid residues in the selected models were located in favoured locations for both MT and SoDIT-a proteins, whereas only 5.8% and 5.4% or 2.2% and 0.0% of the amino acid residues were in allowed sites or disallowed

regions, respectively. Thus, the calculation of conformational energy enabled the prediction and determination (at 99.7% (MT) and 99.8% (SoDIT-a)) of 3D structures with the target model amino acid sequences, and the PROCHECK results suggested that predicted models are accurate and of good quality. The ERRAT score for MT and SoDIT-a protein models were calculated to be 97.721 and 98.256, respectively, indicating a high accuracy of the structure prediction (Figure 4c,d). Based on these results and the N-terminal and C-terminal residues of the tested proteins, the ERRAT values showed high flexibility and high stereochemical plausibility.

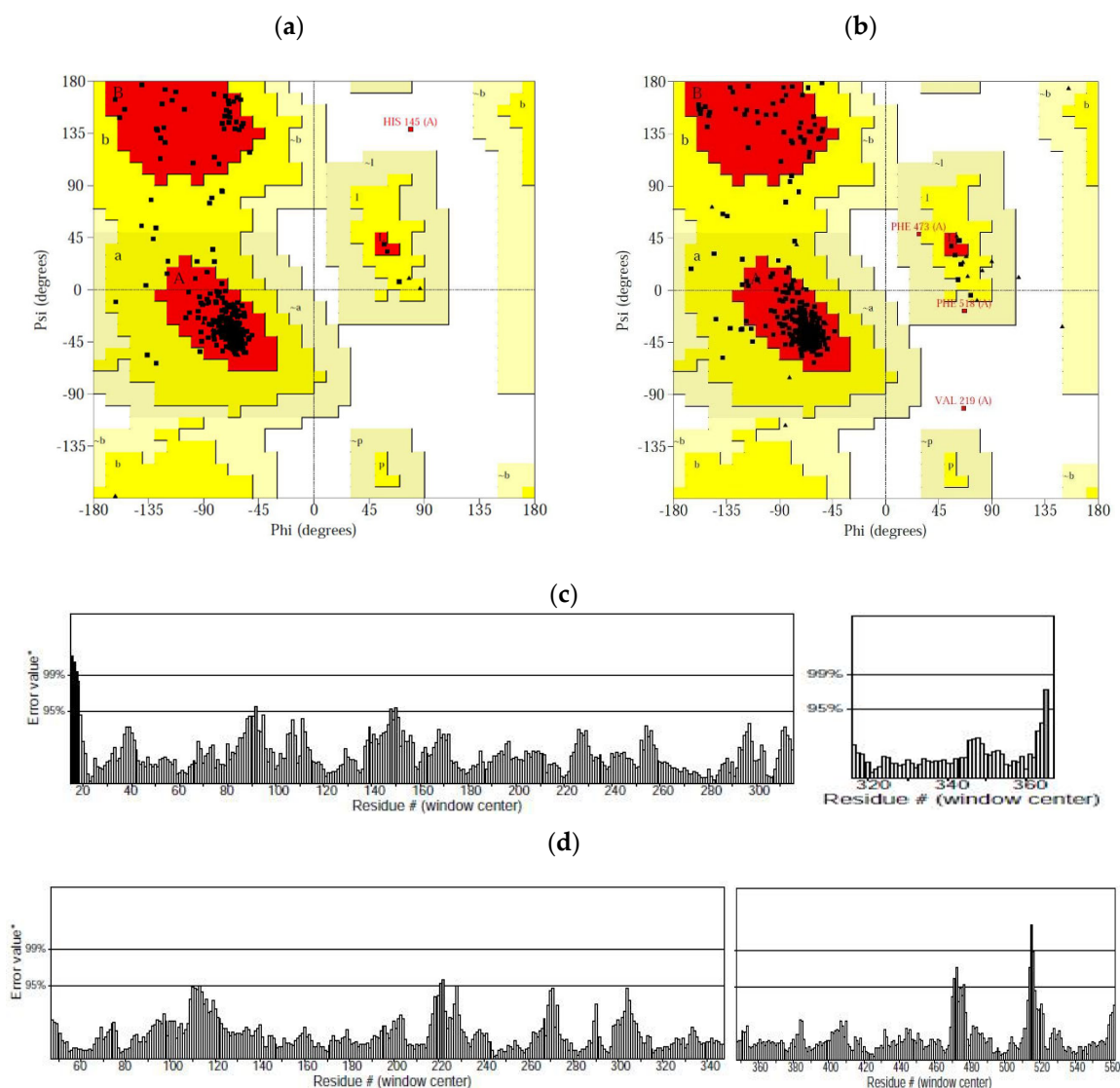


Figure 4. Model validation and Ramachandran plot analysis of tested proteins (as analysed by RAMPAGE) for (a) MT and (b) SoDIT-a models, as well as ERRAT analysis of (c) MT and (d) SoDIT-a proteins.

2.4. Molecular Docking Analysis

To explain the transport mechanisms of certain acids in MT and SoDIT-a proteins, it is necessary to explore their binding mode structures. Therefore, docking was performed using AutoDock Tools with the help of the Genetic Algorithm scheme, and the best-docked structures of citric and malic acids were selected based on the binding energy (-7.27 kcal/mol). The molecular docking results showed a high tendency for amino acid residues to be found in the binding pockets. The docked structure predicted interactions of citric and malic acids with the neighbouring residues in the MT active site (such as LEU230,

GLY231, and ALA305) that correlated well with our predicted interacting studies (Figure 5) and leading to citric acid being more stable than malic acid in the active binding pocket. The differences in binding affinity/mode for the docked ligands were described in Table 1.

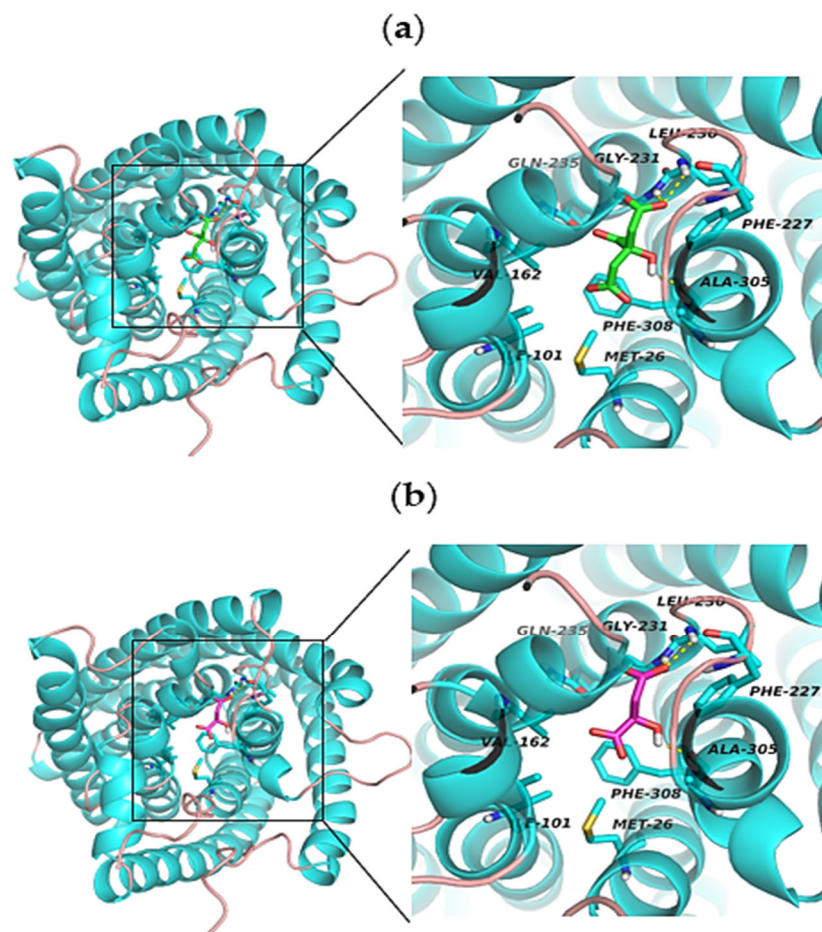


Figure 5. Active site interacting residues of modelled MT protein form in the docked structure with (a) greenish-blue and green colour ribbons representing modelled MT with citric acid, or (b) greenish-blue and red colour ribbons representing modelled MT with malic acid, respectively.

Table 1. Binding energies of docked ligands.

Receptors	Binding Energy with Citrate (Binding Energy, kcal/mol)	Binding Energy with Malate (Binding Energy, kcal/mol)
MT	−3.44	−2.85
Sodit-a	−7.27	−6.00

In contrast, the docked structure predicted interactions with the neighbouring residues of citric acid in the SoDIT-a active site were as follows: ASN223, THR224, ALA276, SER475, SER477, THR520, and GLY521, in addition to double hydrogen bond interactions with ASN223, THR224, and SER477—supporting the stability of citric acid (Figure 6a). In contrast, ASN223, THR224, ALA276, SER475, and SER477, in addition to the double hydrogen bond interactions with ASN223, THR224, and SER477, were among the experimentally known key residues that correlated well with our predicted interacting study regarding the SoDIT-a active site of malic acid (not having double hydrogen bond interactions with THR520 or GLY521 (Figure 6b). This resulted in relatively weak binding stability when compared to that of citric acid. By this evidence, our results demonstrated that citric acid has a lower docking binding energy than malic acid.

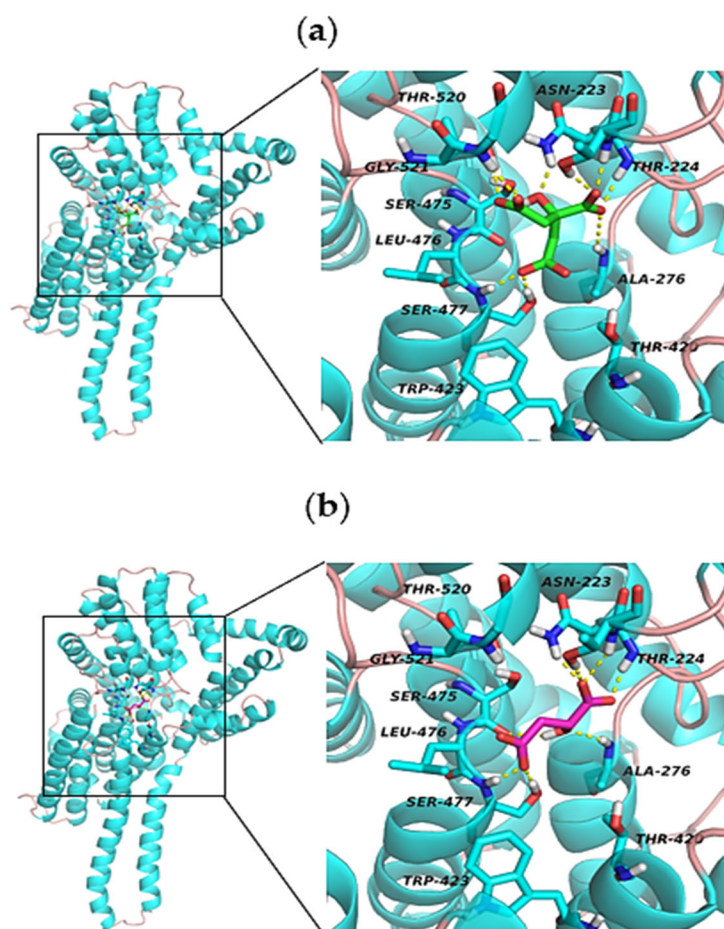


Figure 6. Active site interacting residues of modelled SoDIT-a protein form in the docked structure with (a) greenish-blue and green colour ribbons representing modelled SoDIT-a with citric acid, or (b) greenish-blue and red colour ribbons representing modelled SoDIT-a with malic acid, respectively.

2.5. Molecular Dynamics Simulations

To refine the obtained structure via homology modelling, 10 ns of the simulation was applied, and the production run with its RMSD value was computed and plotted using the XMGRACE tool. As illustrated in Figure 7a, the trajectory of the tested proteins has an overall stable RMSD value of around 0.3~0.4 nm. The radius of gyration values for the trajectory of MT-Citrate and MT-Malate, in addition to SoDIT-a-Citrate and SoDIT-a-Malate, was also determined, and proved to be stable at an average value of 0.2~0.3 to 0.4~0.5 nm over the equilibration course (Figure 7b). The root-mean-square fluctuations (RMSF) plot also demonstrated that the residual level in fluctuations of the studied proteins was minimal, except for the residues located at the terminal (Figure 7c). The time it took for a particular H-bond to form was monitored throughout the simulation and a large number of direct hydrogen bonds between the protein and the ligands of MT-Citrate, MT-Malate, SoDIT-a-Citrate, and SoDIT-a-Malate systems were detected (Figure 7d). These results indicated that the simulation was a stable one and that the generated structures had attained stability.

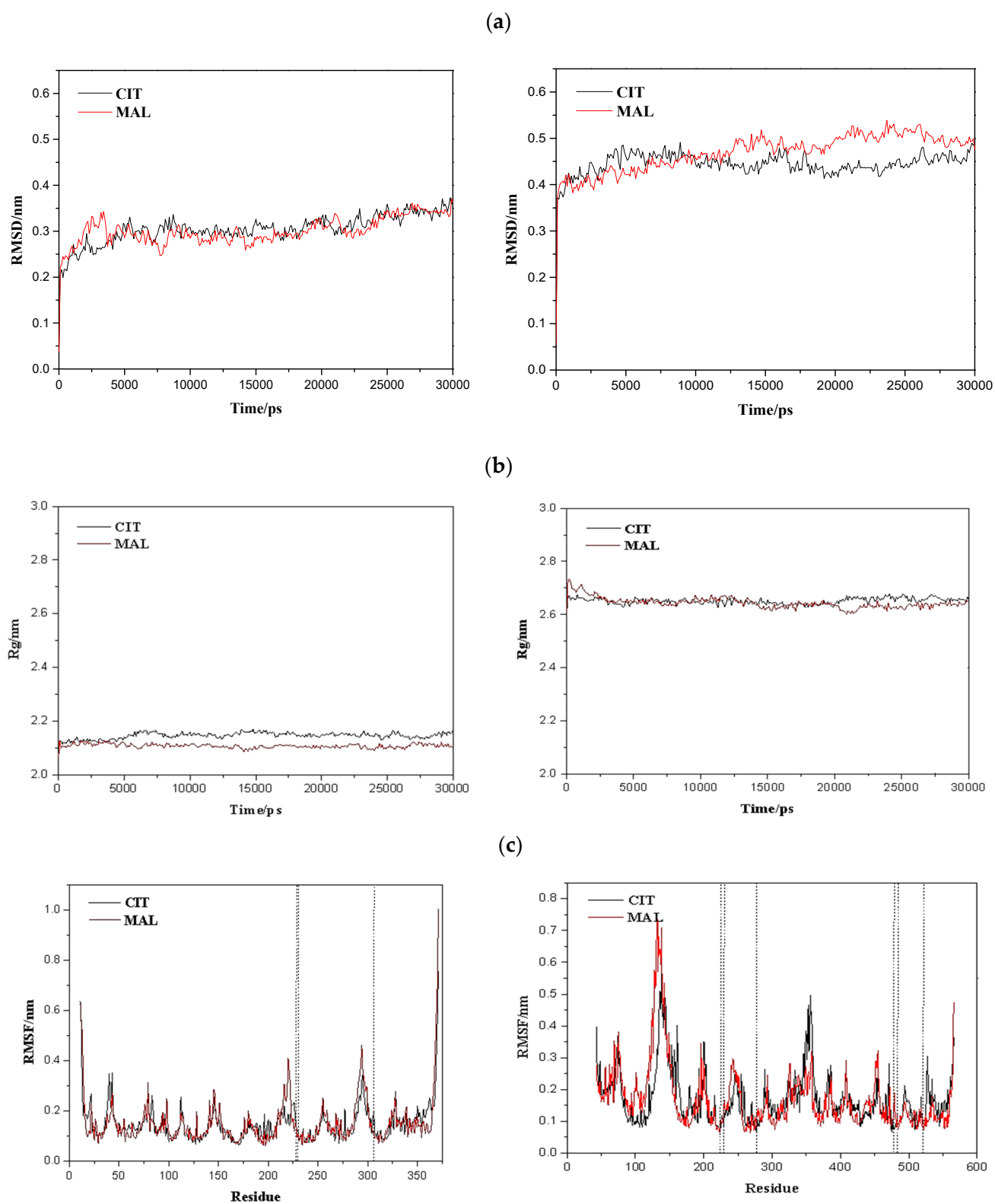


Figure 7. Cont.

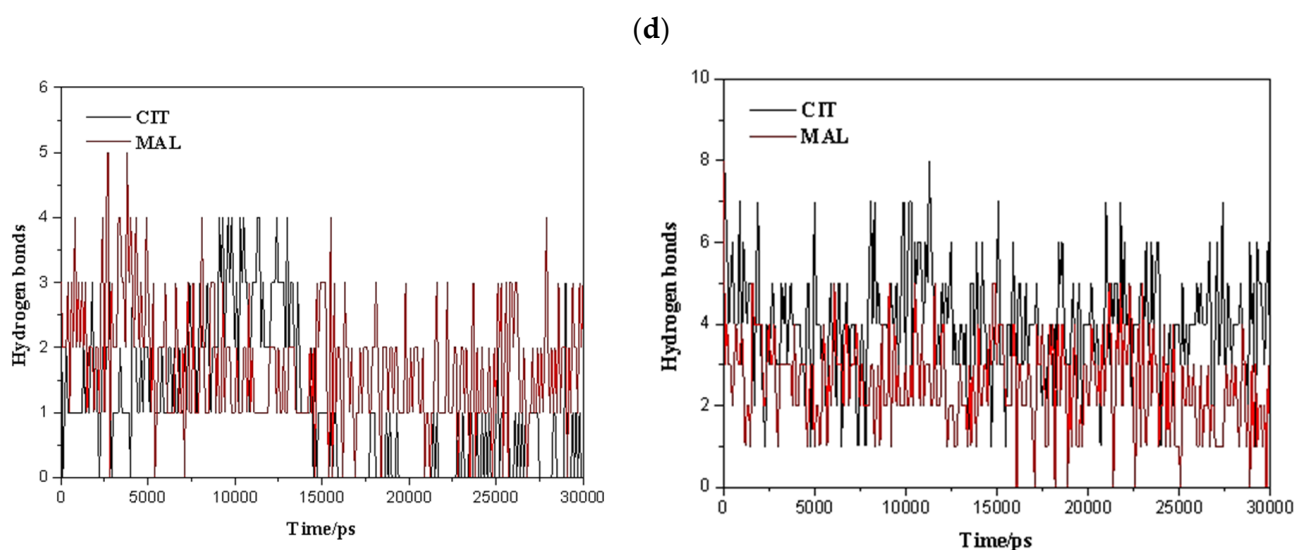


Figure 7. Molecular dynamics simulations showing a stable protein complex. (a) The root mean square deviation (RMSD) of MT-CIT and MT-MAL (left) and SoDIT-a-CIT and SoDIT-a-MAL (right) in the complex over 10 ns in comparison with values for the unbound (free) proteins. (b) The radius of gyration versus time for protein transporter molecules in self-association simulations. (c) The difference in RMSF between bound and free proteins. (d) Number of hydrogen bonds between protein(s) and ligand(s) during the simulation period.

2.6. Characterisation of Conformational Study in Selected Proteins

The conformational structures of target proteins MT-CIT, MT-MAL, SoDIT-a-CIT, and SoDIT-a-MAL were studied for a more detailed comparative analysis. The results indicated that the MT-CIT system did not show significant fluctuations in the secondary structure and that the tertiary protein structure remained largely unchanged. This suggested that the structure of the protein was stable over a wide kinetic simulation. Similarly, the MT-MAL system had also been more stable. Notably, the CIT binding stability of MT protein was less stable than for MAL and presented with some dissociation (only in the case of the CIT system). To further explore the dissociation and binding characteristics of CIT and MAL, the minimum distances between the small molecules and MT proteins were analysed, showing that when at the minimum distances for CIT and MAL, the MT proteins were stable and fluctuated significantly, reaching up to 0.6 and 0.17 nm, respectively. These models were thus more stable during kinetic simulations when there was no dissociation (Figures 8 and 9).

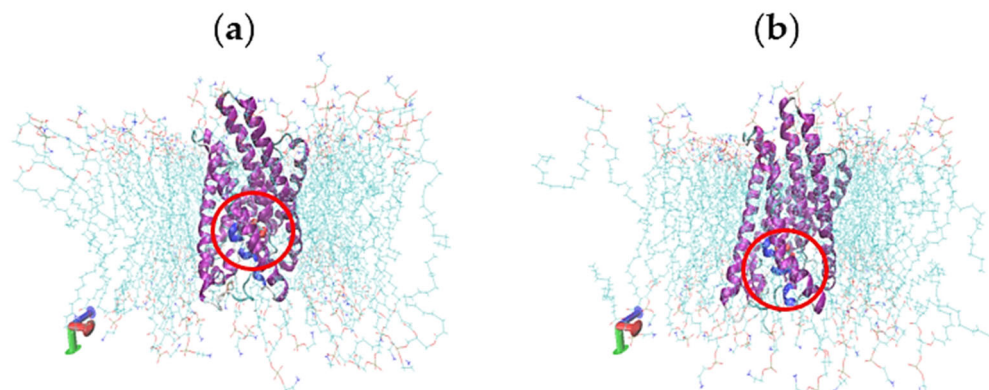


Figure 8. Cont.

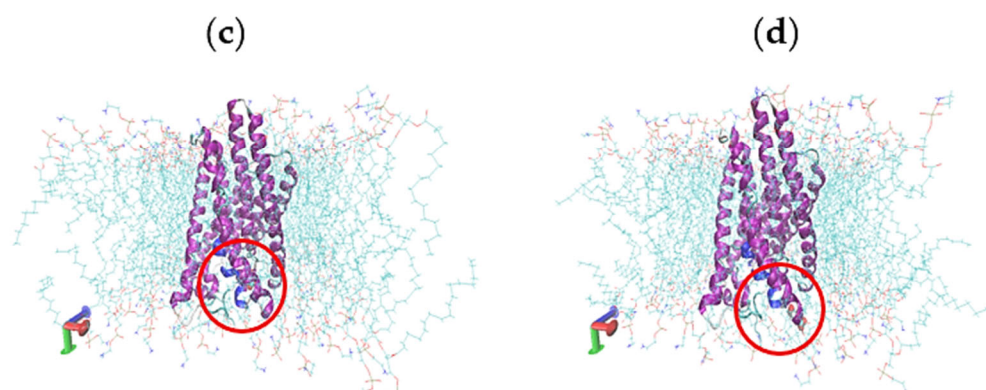


Figure 8. The binding conformations and molecular interaction of MT-CIT system versus molecular dynamics simulation course at (a) 0 ns, (b) 10 ns, (c) 20 ns, (d) 30 ns with MT depicted in the cartoon, membrane indicated with a line, and the ligand drawn as a circle.

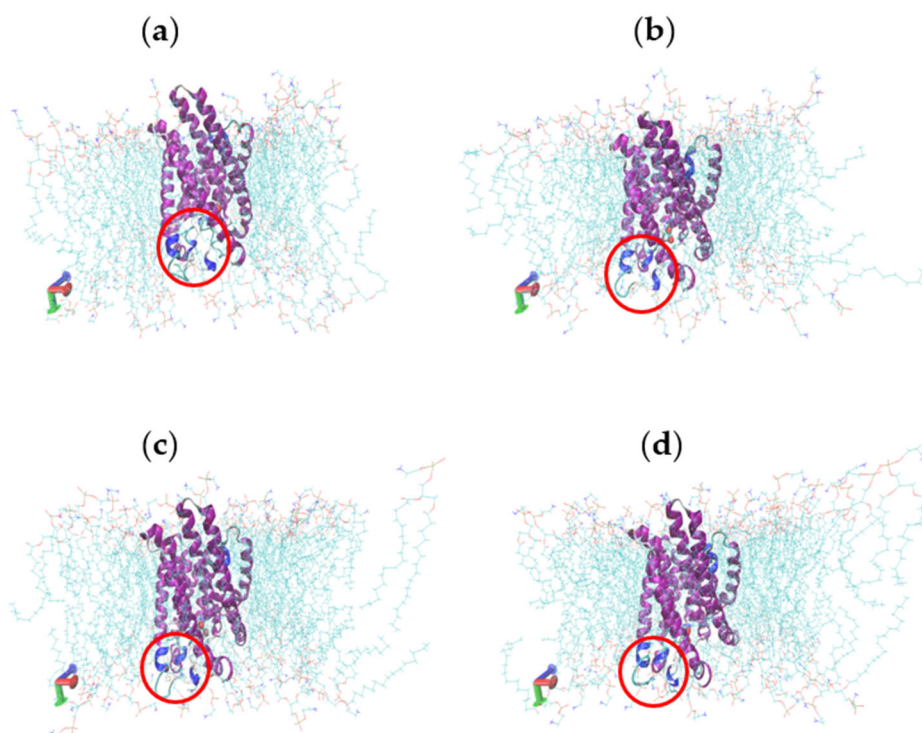


Figure 9. The binding conformations and molecular interaction of MT-MAL system versus MD simulation course. (a) 0 ns, (b) 10 ns, (c) 20 ns, (d) 30 ns, MT was in cartoon, membrane in line, ligand in a circle.

Similarly, the conformational structures of the SoDIT-a-CIT target protein did not show significant fluctuations in the secondary structure, with the tertiary protein structure remaining largely unchanged and appearing stable during the kinetic simulation course. In contrast, there was the further structure of the protein with SoDIT-a-MAL and the stability was improved. Meanwhile, the CIT and MAL binding stability of SoDIT-a proteins were more stable with no dissociation during the kinetic simulation. The minimum distance of MAL in the M1701 protein had been large when compared to CIT, and this may lead to poor binding stability. The secondary structures, in addition to their observed conformational occurrences via the molecular dynamic's simulation, are illustrated in Figures 10 and 11.

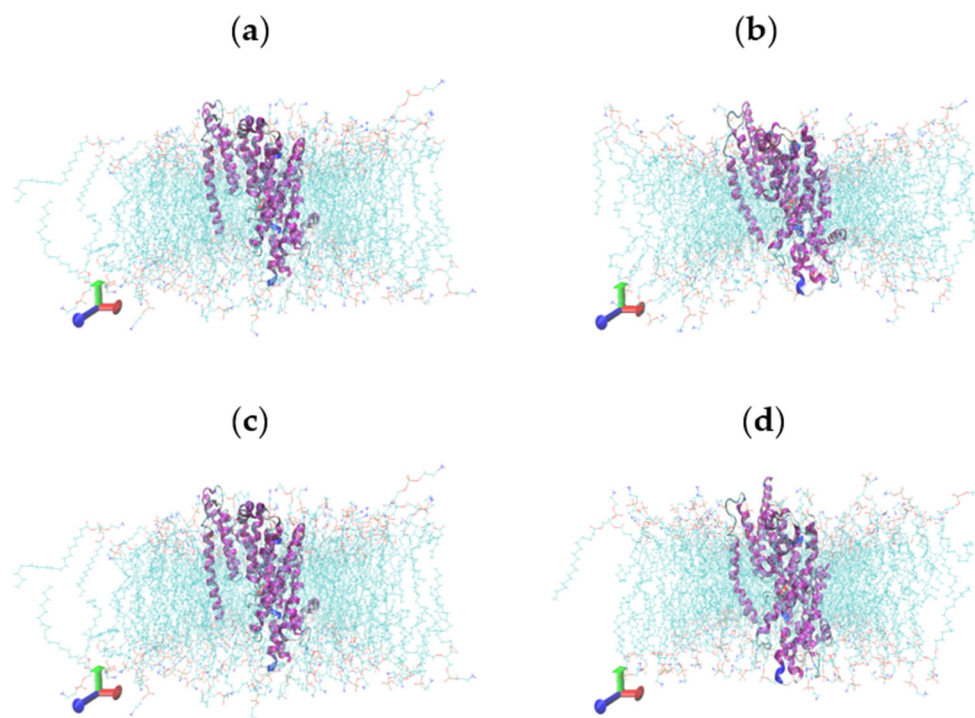


Figure 10. The binding conformations and molecular interaction of SoDIT-a-CIT system versus MD simulation course. (a) 0 ns, (b) 10 ns, (c) 20 ns, (d) 30 ns, SoDIT-a was in cartoon, membrane in line, a ligand in a circle.

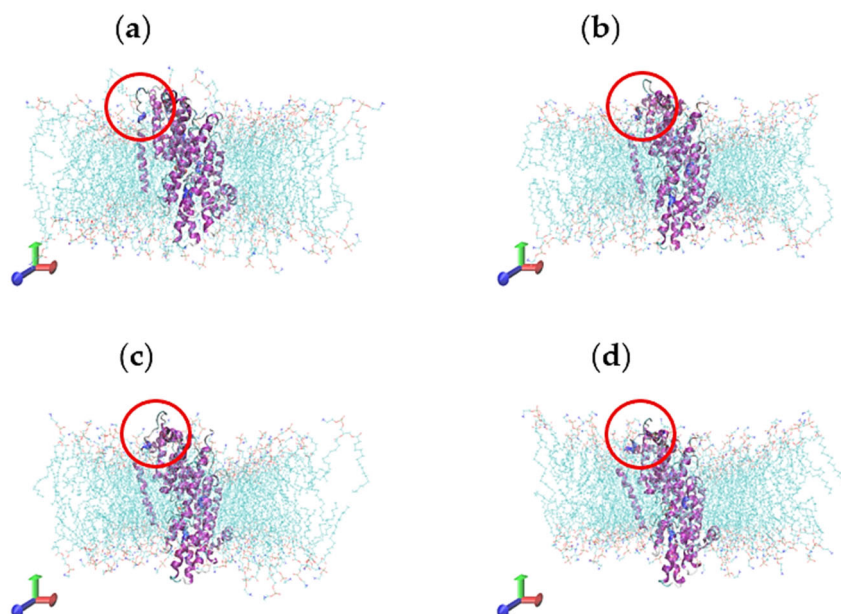


Figure 11. The binding conformations and molecular interaction of SoDIT-a-MAL system versus MD simulation course. (a) 0 ns, (b) 10 ns, (c) 20 ns, (d) 30 ns, SoDIT-a was in cartoon, membrane in line, a ligand in a circle.

2.7. Discussion

Oleaginous microorganisms, mainly fungi, are known for their high lipid contents and are thought to be promising cell factories for the production of high-value FAs. Because of this, these fungi have become industrial targets for different lipid products [14,15], and metabolic engineering approaches have been used to try and enhance their lipid and FA

contents [16]. It has been established that malate accumulation in the cytosol could result in the production of citric acid (due to an exchange of malate and citrate across the fungal mitochondrial membrane) [4,10]. Therefore, it has been predicted that the mitochondrial malate transport system plays a significant role in lipid production by regulating malate flux between the mitochondrion and the cytoplasm, with some studies have reported on this mechanism in oleaginous microorganisms [10].

To fully understand a protein's biological function, it is necessary to know more than just its primary sequence or even its secondary structure, and it is critical to know its tertiary structure. Yet, 3D structures of malate transporter proteins have not been reported in the PDB database. In our ongoing research on mitochondrial transporters, we have identified 51 transporter genes that were predicted to be concerned with a variety of essential metabolic pathways, including oxidative phosphorylation, FA oxidation, the TCA cycle, and the degradation of amino acids. In previous research, we found that fungal strain WJ11 contained two 2-oxoglutarate/malate antiporter genes (SoDIT-a and b) and one MT gene for transporters of the mitochondrial malate transport system [12].

Based on known genomics data of *M. circinelloides* WJ11, including nucleotide sequences and phylogenetic analyses, this strain was selected as a model organism to study the malate transport system. Target proteins (MT and SoDIT-a) were classified to be stable based on their amino acid residues and GRAVY values. Similar to our current findings, the predicted GRAVY value of DTP1 (a modelled divalent transporter protein) demonstrated the sum of hydropathy and GRAVY values of all amino acids, confirming that the target protein showed a higher hydrophobic rather than hydrophilic nature [17]. In addition, the GRAVY Index of glutathione reductase of *Streptococcus thermophilus* (GRst) was estimated to be equal to -0.074 , confirming its solubility consistency in the current study [18]. When it comes to proteins, it is possible to look at the aliphatic index (i.e., the volume occupied by amino acids with an aliphatic side chain such as alanine, valine, isoleucine, and leucine) as the positive factor for globular proteins' thermal stability [19].

The physico-chemical properties of a specific protein sequence can also classify various parameters that aid in the elucidation of protein stability [19,20], purification [21], and functionality [22]. Recent studies have indicated that physico-chemical analyses may reveal, for example, high polar residues of glutathione reductase of *Streptococcus thermophilus* (GRst), including glutamine (7.1%), threonine (7.3%), glycine (10.7%), as well as 3-cysteine residues, which support the enzyme's disulphide bridges and its hydrophilic characteristic [23]. The expected physio-chemical features highlighted the reliability, stability, and efficacy of the potential model structures of MT and SoDIT-a proteins, and these models were therefore tested for further validation. The most dependable and beneficial means for predicting protein configuration is via homology modelling. It enables the prediction of geometrical structures of individual and/or multiple template proteins (if enough sequence identities are provided). When the sequence identity between the target proteins and their templates obtain a high-reaching sufficient, the simulation might even be enough exact to carry out structure-based protein analyses [24,25]. The 3D structure determination of any protein has become the initial and important step in numerous aspects of recent medical and biological research [26].

In the current study, MT and SoDIT-a, two mitochondrial malate transporter proteins in an oleaginous fungal strain WJ11, were considered biologically important transmembrane proteins, although no previous studies have characterised their 3D structures. Based on the hydrophobic nature of transmembrane proteins, the complete prediction of their purification, expression, and crystallisation is difficult due to the numerous and complex natures of such proteins. Consequently, the 3D structure determination of these studied proteins through experimental approaches is highly challenging [27].

In several reports, the TASSER technique has been considered one of the best knowledge-based approaches regarding the structural improvement of proteins [28–30]. An earlier study set out to improve the purification and refinement of protein structures by using a repetitive implementation of the TASSER assembly procedure, creating the novel

I-TASSER procedure [31]. For example, the 3D structure of beta-(1,3)-endoglucanase ENGL1 protein (Q9UVV0) from *Aspergillus fumigatus* was submitted to homology modelling using the I-TASSER server, and predictions were made after a PROCHECK analysis with multiple templates [32]. By following these procedures, the structures were revealed to find close interactions among the atoms. Typically, when more than 90% of amino acid residues are located in the 'allowed' regions, the stereo-chemical quality of the protein would be high [33,34]. Similar to our findings, a recent study indicated that the stable nature of the stereo-chemical and their secondary structural elements of the response regulator (GacA) and transcriptional activator (RhIR) protein models have been reported via Ramachandran plot by using PROCHECK, and results demonstrated that 95.3 and 97.2% residues, respectively, related to most favoured sites and no residual levels located in the disallowed region of the plot [35].

When the protein sequences have a sequence identity lower than 30%, potential alignment errors may also appear in the 3D structure prediction [36,37]. Nevertheless, the percentage identity between MT and SoDIT-a proteins and their best template sequences were very high in our study. Taken together with the findings obtained from the molecular dynamics simulations, ERRAT quality check results, and Ramachandran plot findings, the refined structure was considered to be suitable for further docking analysis and confirmed that the generated models were reliable and of good quality. Docking results indicated that amino acid residues, as presented in Figures 5 and 6, may play a critical role in keeping functional conformation and may furthermore be involved in ligand binding and enhancing the biological activities of the lead molecules [35]. For such an interaction study, the *Euphorbia tirucalli* peroxidase (ETP) model was docked with heme using the AutoDock software. An efficient binding result indicated that the protein could form hydrogen bond networks containing active residues of amino acid, with minimum binding energy and RMSD values reaching up to -8.11 kcal/mol and 0.189, respectively [38]. Moreover, docking studies provided insight into the prediction of the activity, affinity, binding, and orientation of our tested proteins.

To know if the protein is more stable, related to the preliminary secondary structure, and how it may affect its analytical role, the RMSD could be declared (representing an essential property) [39]. Moreover, numerous functioning proteins achieved conformational changes, meaning flexibility will be necessary for the success of their biological activity [40]. The changes of the protein structure and its quantification in the physiological and experimental conditions may be assessed by RMSD factors [23,39], where the crystallographic structure and its ligand geometries can be detected within 2 \AA RMSD and reaching up to 80% would be similar to our docking studies [41]. The ligands pose with the highest score ranged less than 1 \AA in our study.

3. Materials and Methods

3.1. Nucleotide Sequences and Phylogenetic Analysis

The partial nucleotide sequences of two malate transporters (MTs) were first obtained after noting an overexpressed band in our previous research work [12]. The corresponding DNA of the band was subsequently sequenced (encoded by scaffold00018.48 and scaffold00005.20) and compared against the full genome assembly of *M. circinelloides* WJ11 (accession no. CCTCC No. M 2014424), after which complete cDNA sequences, designated as MT and SoDIT-a, were obtained. The respective protein sequences were predicted via Uniprot (<https://www.ncbi.nlm.nih.gov/>, accessed on 23 May 2020) and were aligned, via ClustalW multiple-sequence alignments, to selected reference sequences (obtained from the NCBI protein database).

3.2. Physico-Chemical Properties and Sequence Analysis

Physico-chemical properties of MTs (i.e., amino acid composition, molecular weight, the total number of negatively and positively charged residues, isoelectric point (pI), instability and aliphatic index, and Grand Average of Hydropathy (GRAVY)) were assessed

using the ProtParam tool of ExPASy (<http://web.expasy.org/protparam/>, accessed on 24 May 2020). Hydrophobicity was predicted using ProtScale (<http://web.expasy.org/protscale/>, accessed on 7 July 2020). Protein structure prediction and structure-based function annotations were determined using LOMETS in conjunction with the protein data bank (PDB) database (www.pdb.org, accessed on 17 July 2020) [42]. Protein secondary structures were elucidated using GROMACS 2018 [43].

3.3. Homology Modelling and Validation

The PDB database, via LOMETS, was screened for proteins with similar topology to the target protein sequences (experimentally resolved), and the 3D structures of MT and SoDIT-a proteins were predicted using homology modelling (based on comparative protein structure modelling) and I-TASSER. Thereafter, GROMACS (version 4.6), operated with the Steepest Descent (SD) method, was used for the optimisation of the target proteins, and the 3D models of MT and SoDIT-a were verified using PROCHECK and ERRAT programs followed by sequence alignments (performed with ESPript3.0) [44]. The quality of the obtained models was assessed with PROCHECK and ERRAT analyses. Visualisation of the models was done using the PyMol and VMD programs [45], after which models were evaluated based on Ramachandran plot analysis for comparison and deeper understanding of the secondary structures, as well as evaluated for their overall stereo-chemical properties (using PROCHECK).

3.4. Molecular Docking

The MT and SoDIT-a structures were used as docking targets (constructed by ChemDraw) and analysed for ligand (citric acid and malic acid) binding using AutoDock tools [46]. The number of rotatable bonds for the ligand molecules was set, and hydrogen (including non-polar hydrogen) was combined for further molecular docking simulation calculations. The target protein structures were optimised, and the active site of the transporter protein channel cavity was set. The active site (calculated docking box (grid) size set at $60 \times 60 \times 60 \text{ \AA}$) had a lattice spacing of 0.375 nm with the lattice box centre coordinating with the active site centre (set according to the relevant active site ligand). The number of genetic algorithms (GA) was set to 1000, the number of populations (Population Size) was set to 150, and the maximum number of iterations (Maximum Number of evals) was set to 25,000,000. The structure was energy minimised, and other parameters were used with default values.

3.5. Molecular Dynamics Simulations

The aligned and optimised models were then further analysed using molecular dynamics simulations and small molecules citric acid (CIT) and malic acid (MAL), of which three-dimensional structure files were created using ChemDraw. Combined with the molecular docking results, the minimum energy conformation of the protein-citric acid complex and outputs of molecular dynamics simulations were calculated. GROMACS 2018 was used to create the initial model structures for the transmembrane molecular dynamics simulation. Firstly, the cell membrane-protein-small molecule composite system was built for each protein, based on the energy minimum complex conformation obtained through docking (the cell membrane being a phospholipid bilayer of DOPC and DOPG (7:3)). The cell membrane-transport protein-small molecule complex models were then subjected to a 30 ns molecular dynamics simulation in an aqueous environment system using a GROMACS-based solvent model. The 53a6 GROMOS force field was used with the SPC water model. The simulated system employed a standard cubic box that is wrapped around the model and other molecules, with the complex in the centre of the box. Before subjecting the model to a completely free kinetic simulation, the complex was optimised for 2000 steps using the SD method (to eliminate possible atomic collisions).

Following that, the protein was positioned, and molecular dynamics simulations for the solvent were performed for 100 ps, followed by the protein backbone and ligand

being restricted for 100 ps, and finally, having removed the restriction, the simulation was performed for 100 ps (i.e., the pre-procedure). The simulated system's long-range van der Waals forces were set to 1.4 nm, and the classical interactions were calculated using the spherical 'cut-off' radius method. The simulations were run in steps of 2 fs, with one conformation output every 100 ps and using periodic boundary conditions in all directions. GROMACS 2018 was used to trace the simulations whilst PyMol and VMD were used to visualise them. The root-mean-square deviation (RMSD) can approximate the system's relative change in conformation and is an important criterion for determining whether the simulated system converges. Therefore, in this study, RMSD was used to determine and judge the system's equilibrium.

4. Conclusions

In this study, two genes (encoding MT and SoDIT-a proteins, being potential mitochondrial malate transporters, in the high lipid-producing fungal *M. circinelloides* strain WJ11) were selected and, for the first time, explored to better understand their homology modelling, molecular docking, and dynamics studies. Different parameters were applied whilst assessing their physico-chemical properties. Sequence analysis and further confirmation of expected 3D models via Ramachandran plots revealed that most of the residues were located in allowed and/or favoured regions of the plot. The binding of tested proteins and their active sites were studied using a molecular docking approach. Molecular dynamics simulations confirmed the stability of the tested docked complexes and provided multiple conformational insights regarding their structures. Ideally, findings from this study will stimulate subsequent biochemical investigations of mitochondrial malate transporter proteins, and studying potential substrate-binding locations within a mitochondrial metabolite carrier could further unravel its importance for lipid build-up in oleaginous fungi.

Supplementary Materials: The following supporting information can be downloaded at: <https://www.mdpi.com/article/10.3390/catal13040705/s1>, Figure S1: Prediction of hydrophobicity/hydrophilicity plot analysis of MT protein (A), SoDIT-a protein (B), Whereas hydrophobicity > 0, and hydrophilicity < 0.

Author Contributions: Conceptualization, Y.S., W.Y. and H.M.; methodology, W.Y. and H.M.; software, W.Y. and H.M.; validation, A.M.S. and H.Z.; formal analysis, H.Z.; investigation, A.M.S.; resources, S.P., W.S. and F.X.; data curation, S.P. and W.S.; writing—original draft preparation, W.Y. and H.M.; writing—review and editing, W.Y., H.M. and Y.S.; visualization, A.M.S. and H.Z.; supervision, Y.S.; project administration, Y.S.; funding acquisition, Y.S. All authors have read and agreed to the published version of the manuscript.

Funding: This work was funded by the National Natural Science Foundation of China (grant no. 31972851 and 31670064), TaiShan Industrial Experts Programme (tscy no. 20160101), and Shandong provincial key technology R&D plan (no. 2018GNC110039 and 2018GSF121013).

Data Availability Statement: Not applicable.

Acknowledgments: We thank all staff members in the Colin Ratledge Center for Microbial Lipids, School of Agriculture Engineering and Food Science, Shandong University of Technology for assistance with technical support and software.

Conflicts of Interest: The authors declare no conflict of interest.

References

1. Ochsenreither, K.; Glück, C.; Stressler, T.; Fischer, L.; Syltatk, C. Production strategies and applications of microbial single cell oils. *Front. Microbiol.* **2016**, *7*, 1539. [[CrossRef](#)] [[PubMed](#)]
2. Mohamed, H.; El-Shanawany, A.R.; Shah, A.M.; Nazir, Y.; Naz, T.; Ullah, S.; Mustafa, K.; Song, Y. Comparative Analysis of Different Isolated Oleaginous Mucoromycota Fungi for Their γ -Linolenic Acid and Carotenoid Production. *Biomed. Res. Int.* **2020**, *2020*, 3621543. [[CrossRef](#)] [[PubMed](#)]
3. Mhlongo, S.I.; Ezeokoli, O.T.; Roopnarain, A.; Ndaba, B.; Sekoai, P.T.; Habimana, O.; Pohl, C.H. The Potential of Single-Cell Oils Derived from Filamentous Fungi as Alternative Feedstock Sources for Biodiesel Production. *Front. Microbiol.* **2021**, *12*, 637381. [[CrossRef](#)] [[PubMed](#)]

4. Yang, J.; Li, S.; Kabir Khan, M.A.; Garre, V.; Vongsangnak, W.; Song, Y. Increased Lipid Accumulation in *Mucor circinelloides* by Overexpression of Mitochondrial Citrate Transporter Genes. *Ind. Eng. Chem. Res.* **2019**, *58*, 2125–2134. [[CrossRef](#)]
5. Dong, X.; Chen, X.; Qian, Y.; Wang, Y.; Wang, L.; Qiao, W.; Liu, L. Metabolic engineering of *Escherichia coli* W3110 to produce L-malate. *J. Biotechnol. Bioeng.* **2017**, *114*, 656–664. [[CrossRef](#)]
6. Wang, L.; Zhang, H.; Zhang, Y.; Song, Y. ¹³C metabolic flux analysis on roles of malate transporter in lipid accumulation of *Mucor circinelloides*. *Microb. Cell Fact.* **2019**, *18*, 154. [[CrossRef](#)]
7. Zhu, B.H.; Zhang, R.H.; Lv, N.N.; Yang, G.P.; Wang, Y.S.; Pan, K.H. The Role of Malic Enzyme on Promoting Total Lipid and Fatty Acid Production in *Phaeodactylum tricornutum*. *Front. Plant Sci.* **2018**, *9*, 826. [[CrossRef](#)]
8. Hao, G.; Chen, H.; Du, K.; Huang, X.; Song, Y.; Gu, Z.; Wang, L.; Zhang, H.; Chen, W.; Chen, Y.Q. Increased fatty acid unsaturation and production of arachidonic acid by homologous over-expression of the mitochondrial malic enzyme in *Mortierella alpina*. *Biotechnol. Lett.* **2014**, *36*, 1827–1834. [[CrossRef](#)]
9. Zhang, Y.; Adams, I.P.; Ratledge, C. Malic enzyme: The controlling activity for lipid production? Overexpression of malic enzyme in *Mucor circinelloides* leads to a 2.5-fold increase in lipid accumulation. *Microbiology* **2007**, *153*, 2013–2025. [[CrossRef](#)]
10. Zhao, L.; Cánovas-Márquez, J.T.; Tang, X.; Chen, H.; Chen, Y.Q.; Chen, W.; Garre, V.; Song, Y.; Ratledge, C. Role of malate transporter in lipid accumulation of oleaginous fungus *Mucor circinelloides*. *Appl. Microbiol. Biotechnol.* **2016**, *100*, 1297–1305. [[CrossRef](#)]
11. Huypens, P.; Pillai, R.; Sheinin, T.; Schaefer, S.; Huang, M.; Odegaard, M.L.; Ronnebaum, S.M.; Wettig, S.D.; Joseph, J.W. The dicarboxylate carrier plays a role in mitochondrial malate transport and in the regulation of glucose-stimulated insulin secretion from rat pancreatic beta cells. *Diabetologia* **2011**, *54*, 135–145. [[CrossRef](#)]
12. Yang, J.; Khan MA, K.; Zhang, H.; Zhang, Y.; Certik, M.; Garre, V.; Song, Y. Mitochondrial Citrate Transport System in the Fungus *Mucor circinelloides*: Identification, Phylogenetic Analysis, and Expression Profiling During Growth and Lipid Accumulation. *Curr. Microbiol.* **2020**, *77*, 220–231. [[CrossRef](#)]
13. Xie, Z.R.; Hwang, M.J. Methods for Predicting Protein–Ligand Binding Sites. In *Molecular Modeling of Proteins*; Kukol, A., Ed.; Methods in Molecular Biology, (Methods and Protocols); Humana Press: New York, NY, USA, 2015; Volume 1215. [[CrossRef](#)]
14. Ykema, A.; Bakels, R.H.A.; Verwoert, I.I.G.S.; Smit, H.; van Verseveld, H.W. Growth yield, maintenance requirements and lipid formation in the oleaginous yeast *Apiotrichum curvatum*. *Biotechnol. Bioeng.* **1989**, *34*, 1268–1276. [[CrossRef](#)]
15. Shah, A.M.; Hassan, M.; Zichen, Z.; Yuanda, S. Isolation, characterization and fatty acid analysis of *Gilbertella persicaria* DSR1: A potential new source of high value single-cell oil. *Biomass Bioenergy* **2021**, *151*, 106156. [[CrossRef](#)]
16. Chutrakul, C.; Jeennor, S.; Panchanawaporn, S.; Cheawchanlertfa, P.; Suttiwattanakul, S.; Veerana, M.; Laoteng, K. Metabolic engineering of long chain-polyunsaturated fatty acid biosynthetic pathway in oleaginous fungus for dihomogamma linolenic acid production. *J. Biotechnol.* **2016**, *218*, 85–93. [[CrossRef](#)]
17. Anantram, A.; Janve, M.; Degani, M.; Singhal, R.; Kundaikar, H. Homology modelling of human divalent metal transporter (DMT): Molecular docking and dynamic simulations for duodenal iron transport. *J. Mol. Graph. Model.* **2018**, *85*, 145–152. [[CrossRef](#)]
18. Wilkins, M.R.; Gasteiger, E.; Bairoch, A.; Sanchez, J.C.; Williams, K.L.; Appel, R.D.; Hochstrasser, D.F. Protein identification and analysis tools in the ExpASY server. *Methods Mol. Biol.* **1999**, *112*, 531–552. [[CrossRef](#)]
19. Ikai, A. Thermostability and aliphatic index of globular proteins. *J. Biochem.* **1980**, *88*, 1895–1898. [[CrossRef](#)]
20. Guruprasad, K.; Reddy, B.V.; Pandit, M.W. Correlation between stability of a protein and its dipeptide composition: A novel approach for predicting in vivo stability of a protein from its primary sequence. *Protein Eng. Des. Sel.* **1990**, *4*, 155–161. [[CrossRef](#)]
21. Gill, S.C.; von Hippel, P.H. Calculation of protein extinction coefficients from amino acid sequence data. *Anal. Biochem.* **1989**, *182*, 319–326. [[CrossRef](#)]
22. Bachmair, A.; Finley, D.; Varshavsky, A. In vivo half-life of a protein is a function of its amino-terminal residue. *Science* **1986**, *234*, 179–186. [[CrossRef](#)] [[PubMed](#)]
23. Gholampour-Faraji, N.; Farazmand, R.; Hemmat, J.; Haddad-Mashadrizeh, A. Modeling, stability and the activity assessment of glutathione reductase from *Streptococcus Thermophilus*; Insights from the *in-silico* simulation study. *Comput. Biol. Chem.* **2019**, *83*, 107121. [[CrossRef](#)]
24. Kumar, P.N.; Swapna, T.H.; Khan, M.Y.; Daddam, J.R.; Hameeda, B. Molecular dynamics and protein interaction studies of lipopeptide (Iturin A) on α -amylase of *Spodoptera litura*. *J. Theor. Biol.* **2017**, *415*, 41–47. [[CrossRef](#)] [[PubMed](#)]
25. Jayasimha, R.; Basha, S.; Kotha, P.; Katike, U. Designing, docking and molecular dynamics simulation studies of novel cloperastine analogues as anti-allergic agents: Homology modeling and active site prediction for the human histamine H1 receptor. *RSC Adv.* **2020**, *10*, 4745–4754. [[CrossRef](#)]
26. Xun, S.; Jiang, F.; Wu, Y.-D. Significant refinement of protein structure models using a residue-specific force field. *J. Chem. Theory Comput.* **2015**, *11*, 1949–1956. [[CrossRef](#)]
27. Pasandideh, R.; Dadmanesh, M.; Khalili, S. *In silico* molecular modeling and docking studies on the Leishmania mitochondrial iron transporter-1 (LMIT1). *Comp. Clin. Pathol.* **2020**, *29*, 115–125. [[CrossRef](#)]
28. Boyd, A.; Ciufu, L.F.; Barclay, J.W.; Graham, M.E.; Haynes, L.P.; Doherty, M.K.; Riesen, M.; Burgoyne, R.D.; Morgan, A. A random mutagenesis approach to isolate dominant-negative yeast sec1 mutants reveals a functional role for domain 3a in yeast and mammalian Sec1/Munc18 proteins. *Genetics* **2008**, *180*, 165–178. [[CrossRef](#)]

29. Du, H.; Brender, J.R.; Zhang, J.; Zhang, Y. Protein structure prediction provides comparable performance to crystallographic structures in docking-based virtual screening. *Methods* **2015**, *71*, 77–84. [[CrossRef](#)]
30. Jianyi, Y.; Yang, Z. I-TASSER server: New development for protein structure and function predictions. *Nucleic Acids Res.* **2015**, *43*, 174–181. [[CrossRef](#)]
31. Wu, S.; Skolnick, J.; Zhang, Y. Ab initio modeling of small proteins by iterative TASSER simulations. *BMC Biol.* **2007**, *5*, 17. [[CrossRef](#)]
32. Ahmed, R.; Jain, S.K.; Shukla, P.K. *In-silico* characterization of β -(1,3)-endoglucanase (ENGL1) from *Aspergillus fumigatus* by homology modeling and docking studies. *Bioinformatics* **2013**, *9*, 802–807. [[CrossRef](#)]
33. Morris, A.L.; MacArthur, M.W.; Hutchinson, E.G.; Thornton, J.M. Stereochemical quality of protein structure coordinates. *Proteins Struct. Funct. Bioinf.* **1992**, *12*, 345–364. [[CrossRef](#)]
34. Sariyer, E.; Yakarsonmez, S.; Danis, O.; Turgut-Balik, D. A study of *Bos taurus* muscle specific enolase; biochemical characterization, homology modelling and investigation of molecular interaction using molecular docking and dynamics simulations. *Int. J. Biol. Macromol.* **2018**, *120*, 2346–2353. [[CrossRef](#)]
35. Skariyachan, S.; Ravishankar, R.; Gopal, D.; Muddebihalkar, A.G.; Uttarkar, A.; Praveen PK, U.; Niranjan, V. Response regulator GacA and transcriptional activator RhIR proteins involved in biofilm formation of *Pseudomonas aeruginosa* are prospective targets for natural lead molecules: Computational modelling, molecular docking and dynamic simulation studies. *Infect. Genet. Evol.* **2020**, *85*, 104448. [[CrossRef](#)]
36. Kopp, J.; Schwede, T. Automated protein structure homology modeling: A progress report. *Pharmacogenomics* **2004**, *5*, 405–416. [[CrossRef](#)]
37. Floudas, C.; Fung, H.; McAllister, S.; Mönningmann, M.; Rajgaria, R. Advances in protein structure prediction and de novo protein design: A review. *Chem. Eng. Sci.* **2006**, *61*, 966–988. [[CrossRef](#)]
38. Ankita, S.; Ravi, K.G.; Chikati, R.; Medicherla, V.J. Homology modeling and molecular docking of heme peroxidase from *Euphorbia tirucalli*: Substrate specificity and thiol inhibitor interactions. *J. Mole. Liqu.* **2016**, *220*, 383–394. [[CrossRef](#)]
39. Kuzmanic, A.; Zagrovic, B. Determination of ensemble-average pairwise root mean-square deviation from experimental B-factors. *Biophys. J.* **2010**, *98*, 861–871. [[CrossRef](#)]
40. Haspel, N.; Moll, M.; Baker, M.L.; Chiu, W.; Kaviraki, L.E. Tracing conformational changes in proteins. *BMC Str. Biol.* **2010**, *10*, S1. [[CrossRef](#)]
41. Kolb, P.; Irwin, J.J. Docking screens: Right for the right reasons? *Curr. Top. Med. Chem.* **2009**, *9*, 755–770. [[CrossRef](#)]
42. Ul-Haq, Z.; Saeed, M.; Halim, S.A.; Khan, W. 3D Structure Prediction of Human β 1-Adrenergic Receptor via Threading-Based Homology Modeling for Implications in Structure-Based Drug Designing. *PLoS ONE* **2015**, *10*, e0122223. [[CrossRef](#)] [[PubMed](#)]
43. Abraham, M.J.; Murtola, T.; Schulz, R.; Páll, S.; Smith, J.C.; Hess, B.; Lindahl, E. GROMACS: High performance molecular simulations through multi-level parallelism from laptops to supercomputers. *SoftwareX* **2015**, *1–2*, 19–25. [[CrossRef](#)]
44. Robert, X.; Gouet, P. Deciphering key features in protein structures with the new ENDscript server. *Nucleic Acids Res.* **2014**, *42*, 320–324. [[CrossRef](#)] [[PubMed](#)]
45. Pettersen, E.F.; Goddard, T.D.; Huang, C.C.; Couch, G.S.; Greenblatt, D.M.; Meng, E.C.; Ferrin, T.E. UCSF Chimera—A visualization system for exploratory research and analysis. *J. Comput. Chem.* **2004**, *25*, 1605–1612. [[CrossRef](#)] [[PubMed](#)]
46. Morris, G.M.; Huey, R.; Lindstrom, W.; Sanner, M.F.; Belew, R.K.; Goodsell, D.S.; Olson, A.J. AutoDock4 and AutoDockTools4: Automated docking with selective receptor flexibility. *J. Comput. Chem.* **2009**, *30*, 2785–2791. [[CrossRef](#)]

Disclaimer/Publisher’s Note: The statements, opinions and data contained in all publications are solely those of the individual author(s) and contributor(s) and not of MDPI and/or the editor(s). MDPI and/or the editor(s) disclaim responsibility for any injury to people or property resulting from any ideas, methods, instructions or products referred to in the content.